Isotopic production cross sections of fragmentation residues produced by ^{18}O ions on a carbon target near 260 MeV/nucleon*

Xiao-Dong Xu(徐晓栋)[1,2] Ya-Zhou Sun(孙亚洲)[1] Shi-Tao Wang(王世陶)[1,2†] Bo Mei(梅波)[3]
Shu-Ya Jin(金树亚)[1,2,4] Xue-Heng Zhang(章学恒)[1,2] Zhi-Yu Sun(孙志宇)[1,2] Yi-Xuan Zhao(赵亦轩)[1,2,4]
Shu-Wen Tang(唐述文)[1,2] Yu-Hong Yu(余玉洪)[1,2] Duo Yan(闫铎)[1] Fang Fang(方芳)[1]
Yong-Jie Zhang(张永杰)[1] Shao-Bo Ma(马少波)[1]

[1]CAS Key Laboratory of High Precision Nuclear Spectroscopy, Institute of Modern Physics, Chinese Academy of Sciences, Lanzhou 730000, China
[2]School of Nuclear Science and Technology, University of Chinese Academy of Sciences, Beijing 100049, China
[3]Sino-French Institute of Nuclear Engineering and Technology, Sun Yat-sen University, Zhuhai 519082, China
[4]School of Nuclear Science and Technology, Lanzhou University, Lanzhou 730000, China

Abstract: The isotopic cross sections of residual nuclei produced in fragmentation reactions of ^{18}O projectiles impinging on a carbon target at energies near 260 MeV/nucleon were measured at the HIRFL facility in Lanzhou (China). A full identification of atomic and mass numbers of fragments was achieved from the determination of their magnetic rigidity, energy loss, and time of flight. The production cross sections for a dozen of nitrogen, carbon, and boron isotopes were determined with uncertainties below 30% for most of the cases. The obtained cross sections for N and B isotopes show a rather good agreement with previous experimental data obtained with different projectile energies. The cross sections for some C isotopes seem to exhibit a dependence on the projectile energy. A comparison of the data and several theoretical model calculations are presented.

Keywords: heavy-ion collisions, projectile fragmentation, isotopic production cross sections

DOI: 10.1088/1674-1137/ac827c

I. INTRODUCTION

Fragmentation reactions play important roles in various scientific research fields. Firstly, the projectile fragmentation is one of the most important methods for the production of exotic nuclei. It has been widely used to produce the radioactive nuclei far from stability. Especially, it has proven to be a well suited reaction mechanism for producing heavy neutron-rich nuclei [1– 3]. Secondly, it is a powerful means to produce the hypernuclei [4]. Thirdly, fragmentation reactions are often employed to investigate the structure and dynamics of the atomic nuclei [5] and constrain the equation of state of nuclear matter [6]. Fourthly, fragmentation has a crucial impact on the hadron therapy and the space radiation protection [7]. Last but not least, an accurate database of production cross sections is essential for the development of reliable cross section models, which play a crucial role in the design of radioactive ion beam experiments. For decades, several kinds of theoretical models and empirical formulas have been developed to describe fragmentation reactions, such as the abrasion-ablation model NUCFRG2 [8], modified statistical abrasion-ablation model ABRABLA [9], empirical parametrization EPAX as well as its extensions [10–12], and FRACS code [13–17]. During the development of these theories, large amounts of cross section data obtained in fragmentation reactions have been employed to benchmark and improve their predictive power. Therefore, the investigation of fragmentation reactions and measurement of the production cross sections are crucial. A state-of-art review of projectile fragmentation reaction studies can be found in Ref. [18].

In recent decades, most of the projectile fragmentation reaction studies employed medium or heavy projectiles, such as ^{80}Kr, ^{136}Xe, and ^{238}U. Systematic studies of residual fragments produced with light projectiles are scarce. However, the fragmentation reaction studies using light projectiles are crucial. On the one hand, the peripheral reactions induced by light projectiles have been proved to be useful spectroscopic tools to investigate the structure of nuclei [19]. On the other hand, systematic studies of the residue fragments produced with light pro-

Received 8 June 2022; Accepted 20 July 2022; Published online 24 August 2022

* Supported in part by the National Natural Science Foundation of China (11905260, 12005314), the Western Light Project of Chinese Academy of Sciences, the Heavy Ion Research Facility in Lanzhou (HIRFL), and the open research project of CAS large research infrastructures

† E-mail: wangshitao@impcas.ac.cn

jectiles are important for radiotherapy and space exploration [7]. From a theoretical point of view, the theoretical complexity and limited data lead to a limited predictive power of the model descriptions of the fragmentation reactions induced by light projectiles. Therefore, the experimental data with light projectiles are requested for benchmarking the model calculations. It is also of interest to examine the validity of some widely-used empirical parametrizations (e.g., EPAX3 [12]) in describing the light nuclei.

In this manuscript, we report a set of production cross sections of isotopically separated residue nuclei produced in fragmentation reactions induced by ^{18}O projectiles impinging on a carbon target at energies near 260 MeV/nucleon. This paper is structured as follows. The experimental setup is described in Sec. II. In Sec. III, we present the measured cross sections compared with existing data and the state-of-the-art model calculations. Finally, a summary of the present work is given in Sec. IV.

II. EXPERIMENT SETUP

The experiment was conducted at the HIRFL-CSR facility [20, 21] in Lanzhou (China). The ^{18}O primary beam was transported to the entrance of the second Radioactive Ion Beam Line in Lanzhou (RIBLL2) [22] to impinge on a primary Be target. The main purpose of the experiment was to study the neutron knock-out reactions of C isotopes produced by the fragmentation of ^{18}O projectiles on a primary Be target, and desirable results have been obtained [23, 24]. In the experiment, we also took some measurements in which the primary Be target was removed, and the ^{18}O primary beam was transported through the RIBLL2 beamline and delivered into the External Target Facility (ETF) where the reaction target was located. The details are described as follows.

Fig. 1 is a schematic layout of the RIBLL2 beamline and ETF terminal together with the employed detectors. During the experiment, an ^{18}O beam with an intensity of approximately 10^6 particles per second was accelerated to 280 MeV/nucleon and injected into the entrance of the RIBLL2 beamline. The RIBLL2 was tuned to transport the ^{18}O beam through the F0 and F1 then reached the ETF to bombard a C target with a thickness of 900 mg/cm^2 and a diameter of 50 mm. The ^{18}O ions have an energy about 260 MeV/nucleon at the center of the C target. The projectile fragmentation reactions occurred and several detectors were utilized to measure the experimental information. At F1, a scintillator detector (i.e., SC1 in Fig. 1) was positioned. Another scintillator (see SC2 in Fig. 1) was located upstream of the reaction target at ETF. These two scintillators served as time-of-flight (TOF) detectors to measure the TOF of ions. Most of the detectors were installed at the ETF area. Upstream of the reaction target, a MUlti-Sampling Ionization Chamber (see MUSIC1 in Fig. 1) detector sandwiched by two multi-wire drift chambers (i.e., MWDC1 and MWDC2 in Fig. 1) were located. Downstream of the reaction target, a similar setup including another MUSIC detector (see MUSIC2 in Fig. 1) and two MWDCs (i.e., MWDC3 and MWDC4 in Fig. 1) were installed. The sensitive area of the MUSIC2 detector is sufficiently large to cover almost all outgoing residue particles. MUSIC1 and MUSIC2 were employed to measure the energy loss (ΔE) of ions upstream and downstream of the reaction target, respectively. MWDC1 and MWDC2 were used to measure the trajectories of the incoming particles. The particle identification (PID) for the incoming primary beam upstream of the reaction target was achieved by employing the ΔE-TOF method. Downstream of the C target, the trajectories of the outgoing ions were monitored by MWDC3 and MWDC4. Then, the ions were bent by a dipole magnet (see Dipole Magnet in Fig. 1), which has a large gap that can assure a nearly full acceptance of the fragment residues downstream of the reaction target. Downstream of the dipole magnet, an MWDC array [25] consisting of three MWDCs was positioned and a TOF wall (TOFW in Fig. 1) detector was installed at the end. The detailed description of the charged fragment detector system at the ETF can be found in Ref. [26]. With the experimental information obtained by SC2, MUSIC2, the dipole magnet, the MWDC array, and the TOFW, one can reconstruct the

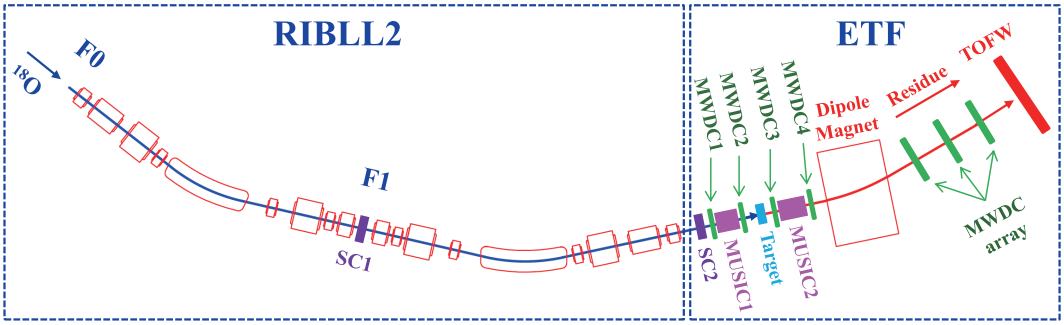

Fig. 1. (color online) Schematic plot of RIBLL2 beam line and the ETF terminal. The detectors used in the experiment are also shown. See text for details.

ion's trajectory, derive the Bρ, and determine the TOF and ΔE. Therefore, the fragmentation residues induced by the ^{18}O projectiles can be unambiguously identified with the so-called $B\rho$-ΔE-TOF method.

Measurements without the reaction target were also conducted with the same beam conditions as the target-in runs. The target-out runs were employed to eliminate the contributions from reactions in the non-target material (e.g., the detection medium, the air gap between detectors). The final cross section was obtained by subtraction of the cross section obtained in the target-out run from that obtained in the target-in run. In order to eliminate the influence of reactions on the target frame, the size of the beam spot on the target was limited by applying a software gate in the off-line analysis.

III. RESULTS AND DISCUSSION

Based on the ETF setup, a general data analysis framework including the data reduction and basic analysis procedures was developed by Y. Z. Sun *et al.* [27, 28]. We employed this framework and conducted a careful data analysis on an event-by-event basis. Particle identification for the ions upstream of the target was obtained. Fig. 2 displays the ion's ΔE measured by MUSIC1 versus the ion's TOF measured by SC1 and SC2. The main cluster corresponds to the ^{18}O ions. Several spots with low statistics are other ion species, which were mainly produced from the interactions of ^{18}O ions with the TOF stop detector, i.e., SC2 in Fig. 1.

For our purpose, the ^{18}O ions upstream of the target were selected. Then, we examined the fragmentation reaction residues induced by the ^{18}O projectiles on the C target. Fig. 3 displays the residue nuclei downstream of the C target. One can clearly see several kinds of ions in this cluster plot. The ion species with the largest intensity corresponds to the ^{18}O ions that passed through the target. In the oxygen isotopic chain, ^{16}O and ^{17}O are also present. Concerning the N, C, and B isotopic chains, in total, there are more than ten isotopes that were produced and can be clearly identified. Beryllium isotopes were also seen in Fig. 3 but with very low statistics. The pileup in the ΔE direction is clearly visible in Fig. 3, especially for the ^{18}O ions. Such pileup signals are attributed to one or multiple ^{18}O ions accidentally intruding to the MUSIC2 detector during its processing of the present signal.

Once the PID for the ions downstream of the target was obtained, one can plot the mass distribution of fragmentation residues, as shown in Fig. 4. It is obvious that the neighboring isotopes are clearly separated, and there are three to four isotopes with relatively sufficient statistics in each isotopic chain.

The production cross section for the fragment residues is calculated as follows:

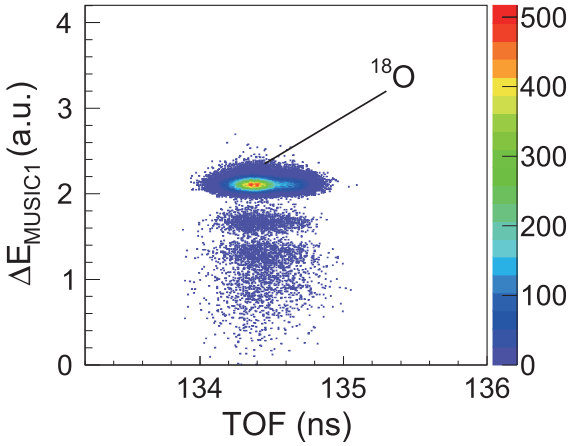

Fig. 2. (color online) Particle identification plot for the ions reached the ETF. The abscissa shows the ion's time-of-flight from F1 to ETF, while the ordinate indicates the ion's energy loss in the MUSIC1 detector.

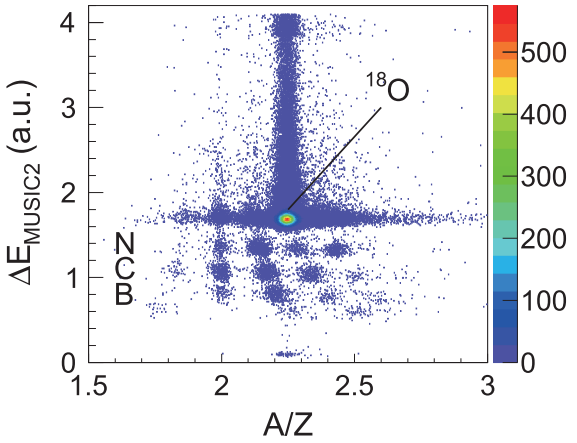

Fig. 3. (color online) Cluster plot of ΔE versus A/Z for the fragmentation residues produced by the ^{18}O ions bombarding on a carbon target at energies near 260 MeV/nucleon.

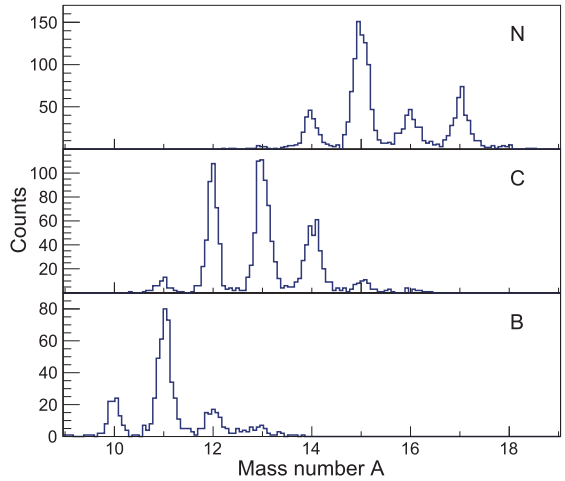

Fig. 4. (color online) Isotopic distribution of nitrogen, carbon, and boron fragment residues.

$$\sigma(A,Z) = \frac{n_f}{n_p n_t \epsilon \eta r}, \quad (1)$$

where n_f, n_p, and n_t are the yields of residue fragments, number of projectiles, and number of target atoms per unit area, respectively. ϵ, η, and r are the geometric acceptance, PID efficiency, and pileup correction coefficient for residue nuclei, respectively. In the following paragraphs, the procedures for the determination of ϵ, η, and r are described.

Concerning the geometric acceptance of the detector setup downstream of the reaction target, the acceptance in the horizontal direction is the main limitation, which is due to the relatively long distance between the TOFW and target. In order to investigate the acceptance of the setup, we carefully examined the ions' horizontal position in the TOF wall detector. It is found that some residue nuclei, namely ^{15,16,17}N, ^{13,14}C, and ^{11}B, are well located within the acceptance range of the TOFW, which indicates that the present setup has a 100% geometric acceptance for these nuclei. However, several isotopes (i.e., ^{14}N, ^{15}C, ^{12}C, ^{12,13}B, and ^{10}B) are not totally accepted by the TOFW. Following similar procedures described in Ref. [29], we fitted the ions' horizontal position distribution by a Gaussian function and used the fitted function to evaluate the missing part of the profile. Then, we calculated the geometric acceptance for each fragment residue.

Regarding the PID efficiency, the measurements using different C beams without the reaction target were employed. The PID efficiency was deduced by comparing the counts of ions that were identified upstream of the target and the number of outgoing ions that were correctly identified with the PID detectors downstream of the target (including MUSIC2, the big dipole, the MWDC array, and the TOF wall). The PID efficiency results are displayed in Fig. 5. It is evident that the PID efficiency of fragment residues ranges from 0.85 to 0.95. The typical efficiency for B isotopes is slightly smaller than that of C and N isotopes. The uncertainties of B isotopes are slightly large, which is mainly due to the low statistics.

In our data analysis, we assume that the pileup correction coefficient for all the ion species is the same. The measurement without the C target was employed to deduce the pileup correction coefficient. Given the fact that the ^{18}O ions have the highest statistics downstream of the reaction target, the pileup correction coefficient is calculated as the ratio between the number of outgoing ^{18}O ions with normal signal and the counts of total outgoing ^{18}O ions.

Once the geometric acceptance, PID efficiency, and pileup correction coefficient are determined, one can calculate the isotopic production cross sections of fragment residuals using Eq. (1). Table 1 lists the cross section results for the N, C, and B fragments. The cross sections are of the order of several mb to several tens of mb. The uncertainties of measured cross sections include statistical and systematic contributions. It is found that the relative uncertainties of the cross sections are below 30% for most of the isotopes.

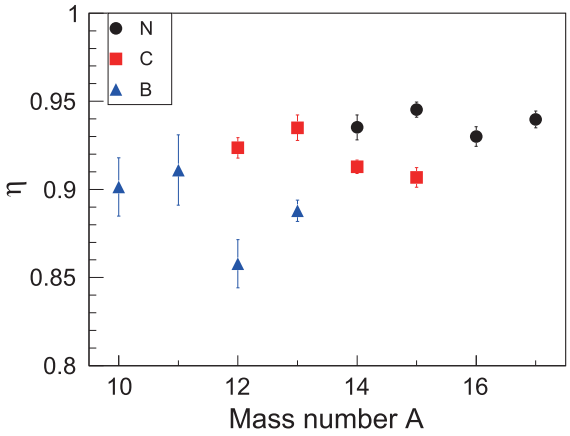

Fig. 5. (color online) The PID efficiency of the setup downstream of the reaction target for N, C, and B isotopes.

Table 1. Isotopic cross sections of nitrogen, carbon, and boron isotopes produced in the reactions of ^{18}O projectiles impinging on a carbon target at energies near 260 MeV/nucleon. Final uncertainties including statistical and systematic uncertainties are also shown.

Z	A	σ/mb	$\Delta\sigma$/mb
7	17	29.12	2.21
7	16	19.89	2.03
7	15	65.16	3.53
7	14	15.80	2.86
6	15	5.03	1.56
6	14	28.50	2.12
6	13	45.63	2.91
6	12	36.32	3.94
5	13	4.14	1.40
5	12	9.05	2.36
5	11	31.25	2.50
5	10	10.48	3.03

In order to compare our cross section results with the previous experimental data obtained from the ^{18}O+^{12}C fragmentation reactions as well as the theoretical model predictions, in Fig. 6, we plotted our data and existing data together with the predictions of EPAX3, FRACS, NUCFRG2, and ABRABLA. The black dots indicate the data obtained in the present experiment with ^{18}O energy at 260 MeV/nucleon. The open squares show the data obtained from the previous experiment performed by Leistenschneider *et al.* with ^{18}O energy at 573 MeV/nucleon [30], while the open triangles indicate the cross sections obtained by another experiment performed by Olsen

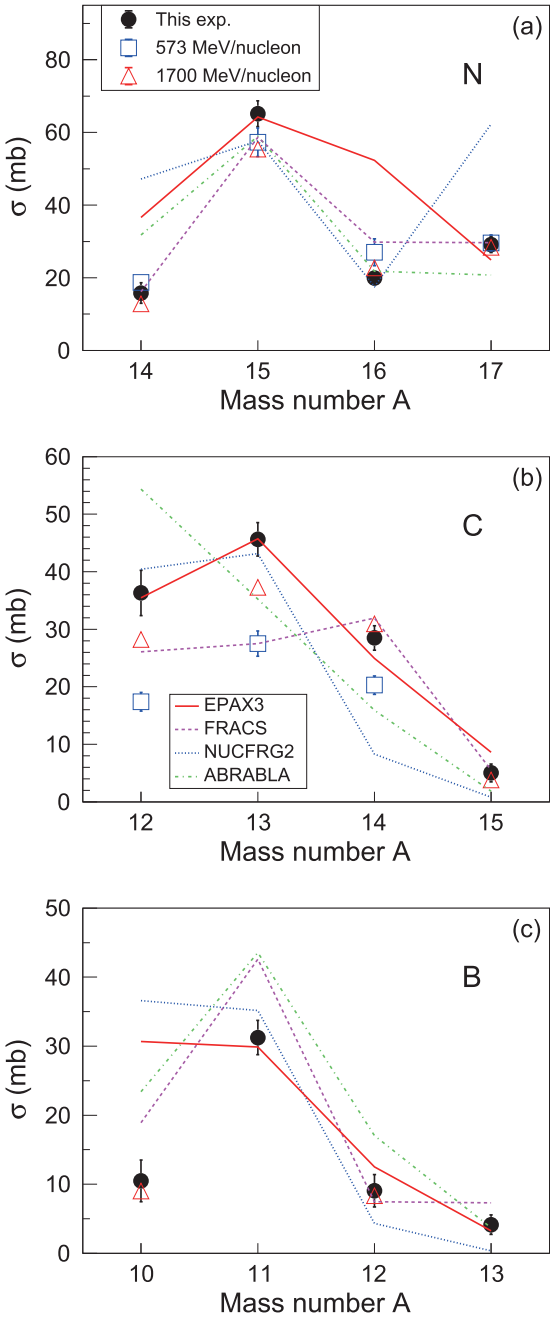

Fig. 6. (color online) Isotopic production cross sections of nitrogen (a), carbon (b), and boron (c) isotopes produced by the ^{18}O + ^{12}C fragmentation reactions. Filled dots indicate the data obtained from the present work, while open squares and open triangles indicate those measured at 573 MeV/nucleon [30] and at 1700 MeV/nucleon [31], respectively. The solid, dashed, dotted, and dash-dotted lines depict the predictions of EPAX3, FRACS, NUCFRG2, and ABRABLA, respectively. See text for details.

et al. with ^{18}O energy at 1700 MeV/nucleon [31]. The theoretical predictions for isotopic production cross section are displayed with different lines. The models used in the present work can be classified into two groups: empirical formulas (i.e., EPAX3 and FRACS) and abrasion-ablation models (i.e., ABRABLA and NUCFRG2). Here, we describe their main characteristics. EPAX3 [12] is the third version of EPAX parametrization [10]. It is a universal empirical formula for predicting the fragmentation cross sections in heavy-ion reactions. The parameters were determined by fitting the experimental cross-section data. The FRACS code [13] was developed on the basis of the EPAX parametrization with several modifications to improve the predictive power. The target and projectile energy dependencies were considered. Later, the odd-even staggering was further incorporated into the FRACS formula [14, 15]. Concerning the ABRABLA model [9], it describes the fragmentation reactions as a two-step process. The first step is the abrasion stage, in which the projectile interacts with the target at the overlapping region and the nucleons abraded from the projectile. In the ablation stage, the pre-fragments de-excite through the evaporation of the light particles. NUCFRG2 [8] is an updated version of the NUCFRG model [32], in which the collisions between projectile and target nuclei are also described by employing an abrasion-ablation picture. The collisions of nucleons are believed to depend on the nuclear density distribution, nucleon-nucleon cross sections, and surface deformation energy of the pre-fragment. This model assumes that the nuclei have uniform nuclear matter distributions. The features of the models described here are brief. A detailed review of these theoretical models can be found in Ref. [18]. In the following, firstly, we discuss the similarities and differences between the data sets displayed in Fig. 6. Then we compare the theoretical calculations with the data.

For the N isotopes, the previous measurements at higher energies are in good agreement with our data. Only for ^{15}N, we observe a small discrepancy, and the uncertainty of the present data is slightly large. Concerning the C isotopes, the situation is slightly complicated. Significant deviations are observed for the cross sections of ^{12,13}C measured by three experiments at different energies. The production cross sections for these two nuclei seem to be energy dependent. This feature is not observed for N and B isotopes. It should be noted that the cross sections of ^{12,13}C measured by the present work have slightly large uncertainties. Future measurements with high precision for the C isotopes are needed to examine the energy dependence and clarify this issue. As for the cross section of ^{14}C, the data measured at 1700 MeV/nucleon beam energy agrees with our result remarkably, while the measurement at 573 MeV/nucleon beam energy provides a smaller value. The situation is similar for ^{15}C, of which the data measured with ^{18}O energy at 1700 MeV/nucleon is in harmony with the present data within uncertainties. Regarding the B isotopes, the present work measured the cross sections for $^{10-13}$B. Our ^{10,12}B data are in quite good agreement with the previous

measurement at 1700 MeV/nucleon beam energy. It is worth mentioning that a prominent feature of the isotopic cross section data shown in Fig. 6 is the odd-even staggering (OES), especially in the case of N residues.

Now, we compare the theoretical model predictions with the data in a qualitative manner. In Fig. 6(a), it is evident that all of the four theoretical predictions roughly reproduce the OES trend of the data. In particular, the FRACS presents an overall reasonable description of the OES strength between neighboring nitrogen isotopes. The calculations with ABRABLA reasonably reproduce the cross sections of ^{15,16}N, while the predictions overestimate the cross section of ^{14}N and underestimate the cross section of ^{17}N. Similarly, the predictions of NUCFRG2 reproduce the ^{15,16}N data but fail to describe the ^{14,17}N data. The EPAX3 calculations reproduce our ^{15,17}N data but strongly overestimate the cross sections of ^{14,16}N. Regarding the model calculations for the cross sections of C isotopes, all of the four model predictions differ drastically, as shown in Fig. 6(b). EPAX3 provides an overall best description of our data with a small underestimation of the cross section for ^{14}C. The NUCFRG2 predictions reproduce the cross sections of ^{12,13,15}C obtained by our measurements within the uncertainties but underestimate the cross section of ^{14}C. The ABRABLA predictions illustrate a monotonic decrease in cross sections and fail to describe the trend of data from ^{12}C to ^{15}C. FRACS provides a reasonable description of the cross sections for ^{14,15}C but significantly underestimates the cross sections of ^{12,13}C obtained by the present work. In Fig. 6(c), the EPAX3 and the NUCFRG2 predictions show a similar trend, which greatly overestimates the cross section of ^{10}B and generally reproduces the cross sections of ^{11,12,13}B. FRACS overestimates the cross sections of ^{10,11}B but offers a reasonable description of the ^{12,13}B data. ABRABLA provides a significant overestimation of the cross sections of ^{11,12,13}B, while its prediction for ^{13}B agrees well with the data.

IV. SUMMARY

Nuclide production cross sections were measured for a dozen of residues produced in the fragmentation of a 260 MeV/nucleon ^{18}O beam on a C target. The measured cross sections of N and B isotopes are in good harmony with previous experimental data. The production cross sections of some C isotopes (especially ^{12,13}C) seem to depend on the projectile energy. Future experiments and improved theoretical models are needed for better understanding of this phenomenon. The data are also compared to several theoretical model predictions. The similarities and differences between the data and calculations are qualitatively discussed.

ACKNOWLEDGMENTS

The authors thank the staffs in the accelerator division of Institute of Modern Physics for providing stable beams.

References

[1] J. Benlliure *et al.*, Nucl. Phys. A **660**, 87-100 (1999)
[2] J. Kurcewicz *et al.*, Phys. Lett. B **717**, 371-375 (2012)
[3] T. Kurtukian-Nieto *et al.*, Phys. Rev. C **89**, 024616 (2014)
[4] T.R. Saito *et al.*, Nucl. Phys. A **881**, 218-227 (2012)
[5] M.V. Ricciardi *et al.*, Nucl. Phys. A **733**, 299-318 (2004)
[6] J. Pochodzalla *et al.*, Phys. Rev. Lett. **75**, 1040 (1995)
[7] C. Zeitlin and C. La Tessa, Frontiers in Oncology **6**, 65 (2016)
[8] J. Wilson *et al.*, Nucl. Instrum. Methods Phys. Res., Sect. B **94**, 95-102 (1994)
[9] J.-J. Gaimard and K.-H. Schmidt, Nucl. Phys. A **531**, 709-745 (1991)
[10] K. Sümmerer *et al.*, Phys. Rev. C **42**, 2546 (1990)
[11] K. Sümmerer and B. Blank, Phys. Rev. C **61**, 034607 (2000)
[12] K. Sümmerer, Phys. Rev. C **86**, 014601 (2012); Phys. Rev. C **87**, 039903(E) (2013) (erratum).
[13] B. Mei, Phys. Rev. C **95**, 034608 (2017)
[14] B. Mei, X. L. Tu, and M. Wang, Phys. Rev. C **97**, 044619 (2018)
[15] B. Mei, Phys. Rev. C **103**, 044610 (2021)
[16] Y. D. Song *et al.*, Nucl. Sci. Tech. **29**, 96 (2018)
[17] C. W. Ma *et al.*, Chin. Phys. C **46**, 074104 (2022)
[18] C. W. Ma *et al.*, Prog. Part. Nucl. Phys. **121**, 103911 (2021)
[19] P.G. Hansen and J.A. Tostevin, Annu. Rev. Nucl. Part. Sci. **53**, 219-61 (2003)
[20] W. Zhan *et al.*, Nucl. Phys. A **805**, 533c-540c (2008)
[21] J. Xia *et al.*, Nucl. Instrum. Methods Phys. Res., Sect. A **488**, 11-25 (2002)
[22] B.-H. Sun *et al.*, Sci. Bull. **63**, 78-80 (2018)
[23] Y. Z. Sun *et al.*, Phys. Rev. C **99**, 024605 (2019)
[24] Y. Z. Sun *et al.*, Phys. Rev. C **104**, 014310 (2021)
[25] Y. Z. Sun *et al.*, Nucl. Instrum. Methods Phys. Res., Sect. A **894**, 72-80 (2018)
[26] Y. Z. Sun *et al.*, Nucl. Instrum. Methods Phys. Res., Sect. A **927**, 390-395 (2019)
[27] Y. Z. Sun *et al.*, Nucl. Phys. Rev. **37**, 742 (2020)
[28] Y. Z. Sun *et al.*, Nucl. Instrum. Methods Phys. Res., Sect. A **985**, 164682 (2021)
[29] Y. Z. Sun, *Study of Single Proton Knockout from* ^{16}*C*, Ph.D. Thesis (University of Chinese Academy of Sciences, 2019) (in Chinese)
[30] A. Leistenschneider *et al.*, Phys. Rev. C **65**, 064607 (2002)
[31] D. L. Olson *et al.*, Phys. Rev. C **24**, 1529 (1981)
[32] J. Wilson *et al.*, Nucl. Instrum. Methods Phys. Res., Sect. B **18**, 225231 (1987)